Climate Dynamics (2022) 59:3175–3191
https://doi.org/10.1007/s00382-022-06237-w

The synergistic effect of the preceding winter Northern Hemisphere annular mode and spring tropical North Atlantic SST on spring extreme cold events in the mid-high latitudes of East Asia

Hao Wang[1] · Fei Zheng[2,3] · Yina Diao[1] · Jianping Li[1,4] · Ruipeng Sun[1] · Xinxin Tang[1] · Yue Sun[1] · Fei Li[1] · Yazhou Zhang[1]

Received: 17 November 2021 / Accepted: 27 February 2022 / Published online: 18 April 2022

Abstract

In this paper, the synergistic effect of the preceding winter positive Northern Hemisphere annular mode (pNAM) and spring negative tropical North Atlantic (nTNA) sea surface temperature anomaly (SSTA) on spring extreme cold events in the mid-high latitudes of East Asia (MHEA) is investigated. The results show that the co-occurrence of the two factors is unfavorable for extreme cold events during spring in the MHEA via the snow cover and atmospheric bridges. Over the Atlantic, the spring nTNA SSTA can lead to an atmospheric response that is similar to the North Atlantic Oscillation, which enhances the persistence of the pNAM and in turn amplifies the negative spring Eurasian snow cover extent (EASCE) anomaly caused by the preceding winter pNAM. Meanwhile, the spring EASCE is closely related to the spring MHEA anomalous anticyclone. In addition to storing its signal in the spring EASCE, the spring nTNA SSTA can also lead to the spring MHEA anomalous anticyclone via the eastward Rossby wave train. The evidence shows that the Rossby wave energy can propagate eastward to the MHEA as a result of the enhanced negative spring EASCE anomaly and Rossby wave induced by the spring nTNA SSTA, and the two factors have an obvious synergistic effect on the spring MHEA anomalous anticyclone. This anomalous MHEA anticyclone becomes a barrier that can hinder the intrusion of cold air from the polar region and can increase the thickness of the atmospheric layer. The anomalous sinking motion of the spring MHEA anomalous anticyclone can also lead to an increase in net radiation received at the surface and increase the air temperature through the vertical motion of air. The southerly wind over the west side of the spring MHEA anomalous anticyclone leads to horizontal warm advection. All of the above processes favor an increase in air temperature and dampen extreme cold events, implying the synergistic effect of the preceding winter pNAM and spring nTNA SSTA on spring extreme cold events in the MHEA.

Keywords Extreme cold events · East Asia · Northern Hemisphere annular mode · North Atlantic · Synergistic effect

1 Introduction

East Asia is among the global regions that are most sensitive to extreme temperatures because it experiences evident climatic fluctuations and has a large population (Easterling 2000; Xin et al. 2013). The mid-high latitudes

✉ Fei Zheng
zhengf35@mail.sysu.edu.cn

✉ Jianping Li
ljp@ouc.edu.cn

Ruipeng Sun
rpsun94@sina.com

[1] Frontiers Science Center for Deep Ocean Multispheres and Earth System-Key Laboratory of Physical Oceanography-Institute for Advanced Ocean Studies-Academy of the Future Ocean, Ocean University of China, Qingdao 266100, China

[2] School of Atmospheric Sciences, Key Laboratory of Tropical Atmosphere-Ocean System, Ministry of Education, Sun Yat-Sen University, Zhuhai 519082, China

[3] Southern Marine Science and Engineering Guangdong Laboratory, Zhuhai 519082, China

[4] Laboratory for Ocean Dynamics and Climate, Pilot Qingdao National Laboratory for Marine Science and Technology, Qingdao 266237, China

of East Asia (MHEA) are mainly semi-arid, and the most important climatic characteristic in this region is its temperature fluctuations, and semi-arid regions are always vulnerable to climate change (Huang et al. 2016). The Rossby wave train brings cold advection downstream and readily causes cold-air outbreaks into East Asia (Joung and Hitchman 1982; Cheung et al. 2012; Park et al. 2014). Extreme cold events occur frequently in this area and, with the accompanying snowstorms and cold rains, they often cause heavy losses to arable and livestock farming, which are the main industries in this region (Chen et al. 2002; Chen et al. 2004; Jeong et al. 2008; Park et al. 2008). Therefore, investigating the interannual variability of extreme cold events in the MHEA and the associated mechanisms is of great importance and may help people better understand and predict these extreme climatic events and reduce the impacts associated with them.

The large-scale atmospheric circulation in the extratropical Northern Hemisphere is dominated mainly by the Northern Hemisphere Annular Mode (NAM), also known as the Arctic Oscillation (AO; Wallace and Gutzler 1981; Thompson and Wallace 1998, 2000; Li and Wang 2003). Several studies have demonstrated that the NAM deforms the Siberian high and then influences the outbreak of cold waves that can further impact the occurrence of East Asian snowstorms (Li and Wu 2012; Screen and Simmonds 2013). The coupled land–atmosphere bridge plays an important part in linking the mid-latitude air temperature with the NAM (Li et al. 2019a). As the Eurasian snow cover anomalies are strongly associated with the NAM, and can persist for a long time, the Eurasian snow cover can store the signal of the NAM and then release it into the atmosphere (Bamzai 2003; Robock et al. 2003; Saito and Cohen 2003; Saito et al. 2004). Yin et al. (2013) showed that the preceding winter NAM is negatively correlated with spring extreme cold events in northeast China via the coupled land–atmosphere bridge (Li et al. 2019a). The NAM is also related to the Siberian high, and the strong westerlies when the positive phase of the NAM develops are a major factor in the weakening of the Siberian high, which can have further impacts on the East Asian climate (Gong and Ho 2002; Gong et al. 2011).

In addition to the NAM, are there other factors that influence the MHEA? Previous studies have found that the North Atlantic can modulate the surface air temperature (SAT) over East Asia through the easterly propagating Rossby wave (Li 2004; Liu et al. 2014; Sun et al. 2015; Wu et al. 2011, 2016; Lin et al. 2016; Li and Ruan 2018; Zhang et al. 2019). Monerie et al. (2017) highlighted the role of the Atlantic sea surface temperature anomaly (SSTA) in predicting the SAT anomaly in the MHEA. Chen et al. (2016) showed that the North Atlantic SST tripole mode is important for the tripole SAT anomalies pattern over the Eurasian continent in spring. Qiao and Feng (2016) found that the North Atlantic SSTA can influence the East Asia trough, which is important in modulating the SAT in the MHEA through the Rossby wave train.

The NAM and Atlantic SSTA can both influence climate variability in the MHEA. However, the synergistic effect of these two factors on influencing the interannual variability of extreme temperatures in East Asia is unknown, and the associated internal mechanism remains unclear. Li et al. (2019a) put forward a new method to examine the synergistic effect of these two factors, and this method has been applied in subsequent studies. For example, Zheng et al. (2021) found that the 2020/21 winter extreme cold event in China was related to the synergistic effect of the 2020/21 La Niña in winter and the warm Arctic. An et al. (2021) revealed the impact of Pacific and Atlantic SSTAs on the SAT anomaly over the Mongolian Plateau and showed that these two factors rely mainly on changing the strength of the circumglobal teleconnection to exert their synergistic effect. Sun and Li (2021) found that wintertime precipitation over southeastern China and the Kuroshio Current in the East China Sea, are significantly enhanced by the synergistic effect of El Niño and the positive phase of the North Pacific Oscillation.

The interannual variability of extreme temperatures in East Asia is of great importance; however, it is rarely investigated. As the NAM in the preceding winter may dampen spring extreme cold events in the MHEA (Yin et al. 2013), and the Atlantic SSTA can also influence the air temperature in East Asia (Qiao and Feng 2016; Monerie et al. 2018), we will focus in this paper on the synergistic effect of the preceding winter positive NAM (pNAM) and the negative tropical North Atlantic (nTNA) SSTA in spring.

The remainder of the paper is organized as follows. Section 2 describes the data and methodology used in this study. Section 3 describes the synergistic effect of the preceding winter pNAM and spring nTNA SSTA on spring extreme cold events and the related atmospheric circulation characteristics in the MHEA, as well as the factors influencing the variability of the spring extreme cold events. The mechanisms related to the synergistic effect are presented in Sect. 4. A summary and discussion follow in Sect. 5.

2 Data and methods

2.1 Data

The datasets used in this study are listed in Table 1. The SST data used here is HadISST1 (version 1.1) provided by the Met Office Hadley Center (Rayner et al. 2003) for the period between 1870 and March 2021 on a 1° latitude × 1° longitude grid. For the extreme temperature indices, we use HadEX3 from the Met Office Hadley Center (Dunn

et al. 2020) to provide the gridded data. The HadEX3 dataset is derived from a number of stations, includes quality control checks, and provides reliable extreme temperature indices. HadEX3 covers the period 1901–2018 on a 1.25° latitude × 1.875° longitude mesh. We used the TNn, TXn, TN10p, and TX10p indices from the HadEX3 dataset, which represent the monthly lowest value of the daily minimum temperature, the monthly lowest value of the daily maximum temperature, the percentage of time when the daily minimum temperature is lower than the 10th percentile, and the percentage of time when the daily maximum temperature is lower than the 10th percentile, respectively. These extreme temperature indices can accurately describe the intensity and frequency of extreme cold events (Dunn et al. 2020). We use the global time series in the HadCRUT4 dataset (from 1850 to January 2021), obtained from the Met Office Hadley Center (Morice et al. 2012), to remove the influence of global warming. To investigate the variability of Eurasian snow cover, the monthly Eurasian snow cover extent (EASCE) time series was obtained from the Global Snow Lab of Rutgers University, which covers the period between 1966 and May 2021 (Robinson et al. 2012). For the spatial distribution of snow cover, the monthly snow cover data from the European Centre for Medium-Range Weather Forecasts (ECMWF) reanalysis version 5 (ERA5) is used, which covers the period from 1950 to November 2021 on a 0.1° latitude × 0.1° longitude grid (Hersbach et al. 2020). We used the National Centers for Environmental Prediction–National Center for Atmospheric Research (NCEP–NCAR) reanalysis dataset for the geopotential height, winds, vertical velocity (omega), air temperature, and sea level pressure (SLP) data (Kalnay et al. 1996). The NCEP–NCAR reanalysis dataset covers the period from 1948 to May 2021 on a 2.5° latitude × 2.5° longitude grid.

As the HadEX3 dataset ends in 2018, and has some missing data over East Asia before 1960, we use the period 1961–2018 for this study.

2.2 Methods

In this paper, we define winter as December–January–February and spring as March–April–May. For example, spring in 2010 covers the period March–May of 2010, and the preceding winter covers December 2009 to February 2010.

We used the two-tailed Student's *t* test to determine statistical significance. To examine whether there is a synergistic effect from two forcing factors F_1 and F_2, we follow the method put forward by Li et al. (2019a). This method can diagnose the joint effects statistically and judge the existence of synergistic effect. Each of the forcing factors can be divided into positive, negative, and neutral phases, and one phase is chosen for each factor. Assuming we select the positive phase for each factor, the condition for each factor can be presented as F_1^+ and F_2^+. $F_1^+F_2^+$ denotes the cases when F_1^+ and F_2^+ both occur, and the related cases are termed as joint events $F_1^+F_2^+$. $F_1^+\backslash F_2^+$ indicates the cases when F_1^+ occurs without F_2^+, and the related cases are termed as single F_1^+ events. In addition, $F_2^+\backslash F_1^+$ denotes cases when F_2^+ occurs without F_1^+, and the related cases are termed as single F_2^+ events. If we study the response (say T) of y to F_1^+ and F_2^+, we can compare the difference between the composite amplifications of different events. If the $|T|$ of $F_1^+F_2^+$ is greater than the maximum of the $|T|$ of $F_1^+\backslash F_2^+$ and $F_2^+\backslash F_1^+$, this indicates that there is a synergistic effect from F_1^+ and F_2^+. Conversely, if the $|T|$ of $F_1^+F_2^+$ is less than the minimum of the $|T|$ of $F_1^+\backslash F_2^+$ and $F_2^+\backslash F_1^+$, this indicates there is an antagonistic effect from F_1^+ and F_2^+. Finally, if the $|T|$ of $F_1^+F_2^+$ is between the $|T|$ of $F_1^+\backslash F_2^+$ and $F_2^+\backslash F_1^+$, this indicates that there is no combined effect from F_1^+ and F_2^+. Therefore, using this

Table 1 Datasets employed in this study

Variable	Period of record	Spatial resolution	Source
SST	1870–3/2021	1° × 1°	HadISST1 (version 1.1) from the Met Office Hadley Center (Rayner et al. 2003)
Extreme temperature indices	1901–2018	1.25° × 1.875°	HadEX3 from the Met Office Hadley Center (Dunn et al. 2020)
Geopotential height, winds, vertical velocity (omega), air temperature and sea level pressure	1949–5/2021	2.5° × 2.5°	National Centers for Environmental Prediction–National Center for Atmospheric Research (NCEP–NCAR) reanalysis version 1 (Kalnay et al. 1996)
Snow cover	1950–11/2021	0.1° × 0.1°	The European Centre for Medium-Range Weather Forecasts (ECMWF) reanalysis version 5 (Hersbach et al. 2020)
The Global SAT time series	1850–1/2021	–	HadCRUT4 from Met Office Hadley Center (Morice et al. 2012)
Eurasia snow cover extent (EASCE) time series	1966–5/2021	–	The Northern Hemisphere snow cover extent climate data record (NH SCE CDR v01r01) from the Global Snow Lab of Rutgers University (Robinson et al. 2012)

method, we can easily judge whether the two influencing factors can generate a synergistic effect.

We also performed dynamical diagnosis by using the Rossby wave ray tracing theory in a horizontally non-uniform basic flow (Li and Li 2012; Li et al. 2015, 2019b, 2021; Zhao et al. 2015, 2019), by means of which the trajectory of the stationary Rossby wave train is traced and the pathway of the impact of the TNA is characterized. As in previous studies (Karoly 1983; Li and Nathan 1997; Li and Li 2012; Li et al. 2015; Zhao et al. 2015, 2019), the dispersion relationship of the Rossby wave frequency and wavenumber in a horizontally non-uniform flow can be written as:

$$\omega = \overline{u}_M k + \overline{v}_M l + \frac{\overline{q}_x l - \overline{q}_y k}{k^2 + l^2}, \tag{1}$$

where ω is the wave frequency; k and l are the zonal and meridional wavenumbers, respectively; $(\overline{u}_M, \overline{v}_M) = (\overline{u}, \overline{v})/\cos\varphi$ is the Mercator projection of zonal and meridional winds; φ is the latitude; $\overline{q} = \nabla_M^2 \overline{\psi}/\cos^2\varphi + f$ represents the absolute vorticity of the background; and $\overline{q}_x$ and $\overline{q}_y$ are the zonal and meridional gradients of $\overline{q}$. Let $K = \sqrt{k^2 + l^2}$ represent the total wavenumber, and the zonal and meridional components of the group velocity take the form:

$$u_g = \frac{\partial \omega}{\partial k} = \overline{u}_M + \frac{(k^2 - l^2)\overline{q}_y - 2kl\overline{q}_x}{K^4}. \tag{2a}$$

$$v_g = \frac{\partial \omega}{\partial l} = \overline{v}_M + \frac{(k^2 - l^2)\overline{q}_x + 2kl\overline{q}_y}{K^4}. \tag{2b}$$

As the background flow changes along the ray, the wavenumbers determined by the kinematic wave theory (Whitham 1960) can be written as:

$$\frac{\mathrm{d}_g k}{\mathrm{d}t} = -\frac{\partial \omega}{\partial x} = -k\frac{\partial \overline{u}_M}{\partial x} - l\frac{\partial \overline{v}_M}{\partial x} - \frac{1}{K^2}\left(l\frac{\partial \overline{q}_x}{\partial x} - k\frac{\partial \overline{q}_y}{\partial x}\right), \tag{3a}$$

$$\frac{\mathrm{d}_g l}{\mathrm{d}t} = -\frac{\partial \omega}{\partial y} = -k\frac{\partial \overline{u}_M}{\partial y} - l\frac{\partial \overline{v}_M}{\partial y} - \frac{1}{K^2}\left(l\frac{\partial \overline{q}_x}{\partial y} - k\frac{\partial \overline{q}_y}{\partial y}\right), \tag{3b}$$

where $\frac{\mathrm{d}_g}{\mathrm{d}t} = \frac{\partial}{\partial t} + \overline{u}_g\frac{\partial}{\partial x} + \overline{v}_g\frac{\partial}{\partial y}$ represents the material derivative moving with the group velocity. According to Eq. (3a, 3b), the zonal and meridional wavenumbers change along the wave ray, which differs from the classic theory (Hoskins and Karoly 1981). Equations (2a, 2b) and (3a, 3b) are termed the wave ray tracing equation set. Therefore, after giving the initial position and zonal wavenumber k, the initial local meridional wave number l can be determined using Eq. (1). Then, the wave ray tracing equation set can be applied to obtaining the corresponding wave ray trajectory. For a large-scale Rossby wave, the integration is terminated when the local meridional wavelength is less than 1000 km.

To investigate the propagation of a stationary Rossby wave, we also calculated the wave activity flux (Takaya and Nakamura 2001). The horizontal wave activity flux is calculated as follows:

$$\mathbf{W} = \frac{p\cos\varphi}{2\left|\overline{\mathrm{U}}\right|}\begin{pmatrix} \frac{\overline{u}}{a^2\cos^2\varphi}\left[\left(\frac{\partial\psi'}{\partial\lambda}\right)^2 - \psi'\frac{\partial^2\psi'}{\partial\lambda^2}\right] + \frac{\overline{v}}{a^2\cos\varphi}\left[\frac{\partial\psi'}{\partial\lambda}\frac{\partial\psi'}{\partial\varphi} - \psi'\frac{\partial^2\psi'}{\partial\lambda\partial\varphi}\right] \\ \frac{\overline{u}}{a^2\cos\varphi}\left[\frac{\partial\psi'}{\partial\lambda}\frac{\partial\psi'}{\partial\varphi} - \psi'\frac{\partial^2\psi'}{\partial\lambda\partial\varphi}\right] + \frac{\overline{v}}{a^2}\left[\left(\frac{\partial\psi'}{\partial\varphi}\right)^2 - \psi'\frac{\partial^2\psi'}{\partial\varphi^2}\right] \end{pmatrix}, \tag{4}$$

where ψ' denotes the perturbation stream function; $\overline{\mathrm{U}} = (\overline{u}, \overline{v})$ represents the climatological mean wind velocity horizontal flow in spring; p is the pressure that is normalized by 1000 hPa; and a represents the Earth's radium.

We use the perturbation hypsometric equation (Li et al. 2021) as follows to investigate the influence of the atmospheric circulation variation on the air temperature:

$$T' = \frac{g_0}{R}\left(\ln\frac{p_1}{p_2}\right)^{-1}\Delta Z'. \tag{6}$$

where T' and $\Delta Z'$ are the anomaly or deviations from their time average between two pressure surfaces p_1 and p_2, respectively, g_0 is the acceleration owing to gravity, and R is the gas constant of dry air. According to Eq. (6), the perturbation mean air temperature of the atmospheric layer is proportional to the perturbation atmospheric thickness bounded by isobaric surfaces. Therefore, the atmospheric thickness anomaly can be applied to represent the perturbation mean air temperature of the atmospheric layer. When the atmospheric thickness is reduced, the mean air temperature of the atmospheric layer drops, and vice versa. We use this perturbation hypsometric equation to investigate the influence of the upper-level atmospheric circulation on the air temperature anomalies.

We defined the NAM index used in this study as the difference in the normalized zonal-mean SLP between 35° N and 65° N (Li and Wang 2003). To exclude the influence of global warming, all variables used in this study are detrended by removing their trends related to global warming.

A dry version of the linear baroclinic model (LBM) is used in this study. The LBM consists of primitive equations linearized about a spring climatology obtained from the NCEP–NCAR reanalysis dataset, and adopts

a T21 horizontal resolution and 20 vertical levels using the sigma coordinate system. The horizontal diffusion has a damping time scale of 0.5 day for the smallest value, and the Rayleigh friction and Newtonian damping have a time scale of (0.5 day)-1 in the lowest three levels and (20 day)-1 in the rest of levels. The further detailed description of the LBM is given in Watanabe and Kimoto (2000). The model is integrated for 30 days. It takes about 20 days for the model to achieve the steady atmospheric circulation, and we use the averaged results of days 26–30.

3 Synergistic effect of the preceding winter NAM and spring TNA SST

Figure 1 shows the correlation maps between the preceding winter NAM and spring extreme temperature indices in East Asia. It can be seen from Fig. 1 that the significant correlation areas for the four extreme cold indices are found across the MHEA. This indicates that when the preceding winter pNAM occurs, the spring daily minimum temperature is usually higher than normal and the number of low-temperature days is less than normal in the MHEA, which further implies that the preceding winter pNAM is unfavorable for the spring extreme cold events in the MHEA (Fig. 1). This result is consistent with the previous study by Yin et al. (2013).

Based on Fig. 1, we select the domain bounded by 40°–60° N and 90°–130° E in the MHEA as the study area. Figure 2 shows the correlation maps between the spring global SSTA and spring area-averaged extreme temperature indices in the MHEA (40°–60° N, 90°–130° E). As shown in Fig. 2a and b, there is a large area in the TNA where the SSTA is significantly positively correlated with TN10p and TX10p simultaneously. This indicates that there are less spring cold days and nights in the MHEA when the spring TNA SST becomes colder. Figure 2c and d shows that the spring TNA SSTA is significantly negatively correlated with both TNn and TXn simultaneously, indicating that when the spring TNA SST becomes colder, the spring minimum temperature in the MHEA is usually higher than normal. The above results imply that the spring TNA SSTA may be another crucial factor with respect to the spring extreme cold

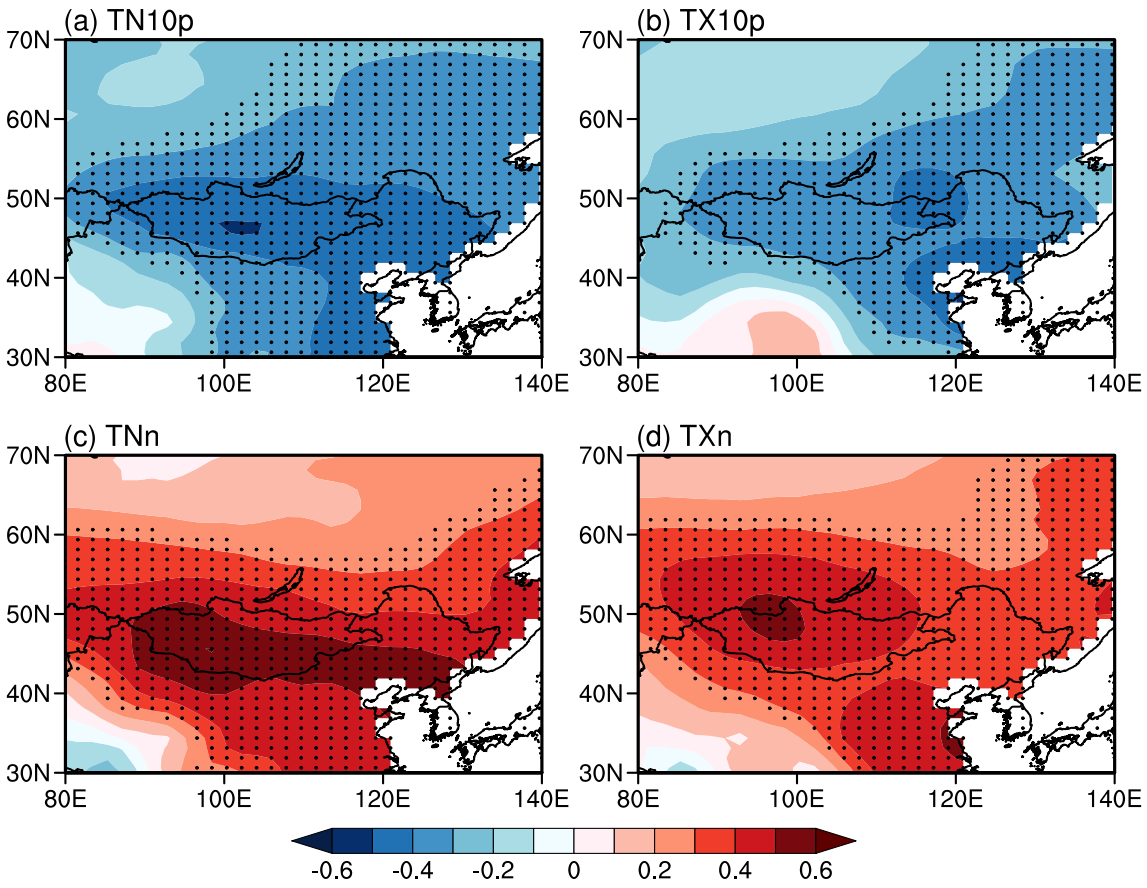

Fig. 1 Correlation maps between the preceding winter NAM and spring extreme temperature indices in East Asia. **a** TN10p. **b** TX10p. **c** TNn. **d** TXn. Dotted areas indicate significant values at the 95% confidence level based on the Student *t* test

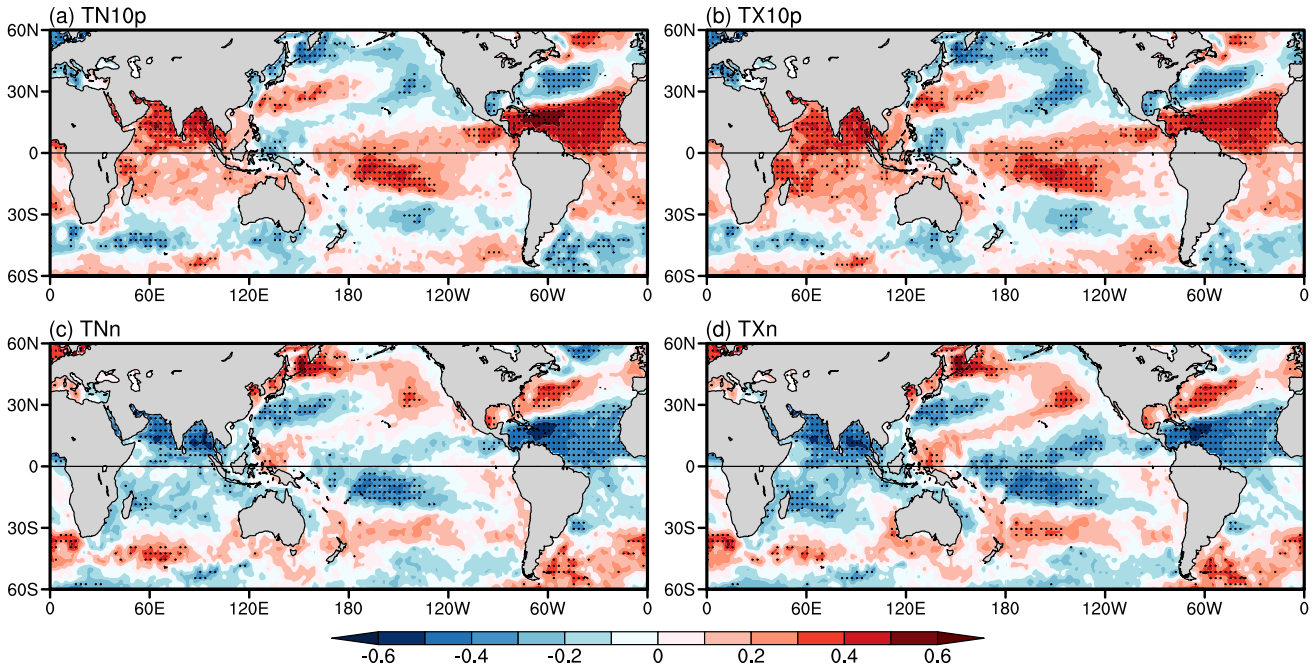

Fig. 2 Correlation maps between the spring global SSTA and spring area-averaged extreme temperature indices in the MHEA (40°–60° N, 90°–130° E). **a** TN10p. **b** TX10p. **c** TNn. **d** TXn. Dotted areas indicate significant values at the 95% confidence level based on the Student *t* test

events in the MHEA. To further quantify the SST variability in TNA, the domain bounded by 0°–20° N and 20°–80° W is selected.

As the preceding winter pNAM and spring nTNA SSTA are both related to the decrease and weakening of the spring extreme cold events in the MHEA, we selected these two factors to investigate whether there is a synergistic effect using the method proposed by Li et al. (2019a). To include more cases in our study, 0.6 standard deviations was used as the threshold to select the preceding winter pNAM and spring nTNA SSTA events. Table 2 lists the numbers and years of the joint events of the preceding winter pNAM and spring nTNA SSTA (pNAM ⊕ nTNA), single preceding winter pNAM events, and single spring nTNA SSTA events. Between 1961 and 2018, there were 7 joint events pNAM ⊕ nTNA, 9 single preceding winter pNAM events, and 9 single spring nTNA SSTA events, and the total number (25 events) accounts for more than one third of all cases across the whole period. This implies that the preceding winter pNAM is not always followed by the spring nTNA SSTA and they are two relatively different factors.

Figure 3a and b shows the time series of the spring area-averaged TN10p and TNn in the MHEA (40°–60° N, 90°–130° E). The magnitudes of most of the spring extreme cold event anomalies in the MHEA for the joint events pNAM ⊕ nTNA are clearly far greater than those for the single preceding winter pNAM or single spring nTNA SSTA events (Fig. 3a, b). For the joint events pNAM ⊕ nTNA, 6 out of 7 are negative (positive) TN10p (TNn) anomalies, and the other is a weak positive (negative) anomaly. However, for the single preceding winter pNAM and spring nTNA SSTA events, only one third show positive TN10p anomalies and, compared with the joint events pNAM ⊕ nTNA, these positive anomalies are relatively weak. This demonstrates that the same-sign rate of the joint events pNAM ⊕ nTNA is much greater than that of the single events, indicating a greater probability of negative extreme cold event anomalies in the MHEA for the cooccurrence of the preceding winter

Table 2 Numbers and years of the joint events of preceding winter pNAM and spring nTNA SSTA (pNAM ⊕ nTNA), single preceding winter pNAM events and single spring nTNA SSTA events

	Joint events of preceding winter pNAM and spring nTNA (pNAM ⊕ nTNA)	Single preceding winter pNAM events	Single spring nTNA SSTA events
Numbers	7	9	9
Years	1975, 1976, 1989, 1990, 2000, 2002, 2008	1973, 1983, 1988, 1992, 1993, 1995, 1999, 2007, 2016	1974, 1985, 1986, 1991, 1994, 2001, 2009, 2014, 2015

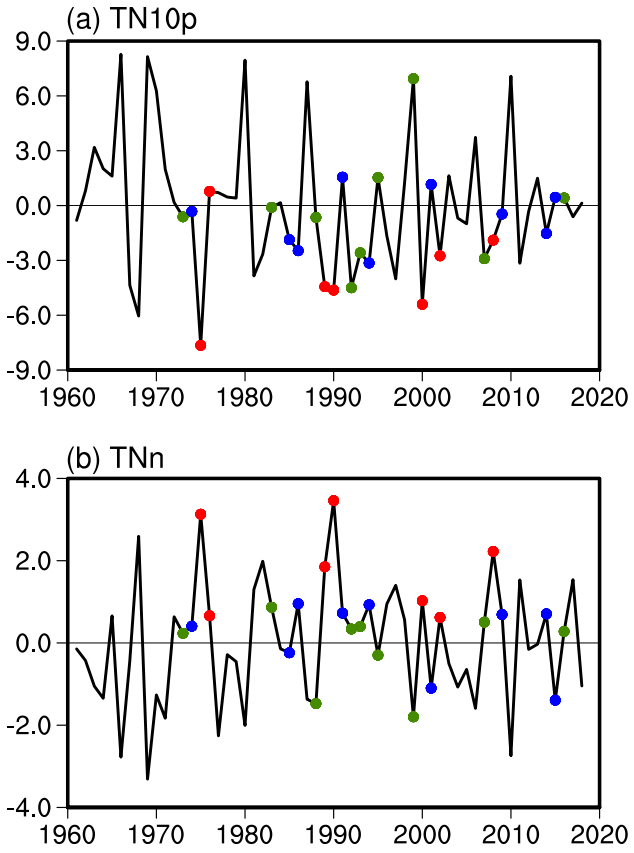

Fig. 3 Time series of the spring area-averaged **a** TN10p (%) and **b** TNn (°C) in the MHEA (40°–60° N, 90°–130° E). The red, green and blue dots represent the joint events of preceding winter pNAM and spring nTNA SSTA (pNAM ⊕ nTNA), single preceding winter pNAM events and single spring nTNA SSTA events respectively

pNAM and spring nTNA SSTA than for the occurrence of only one factor. The composite area-averaged TN10p and TNn anomalies in the MHEA are − 3.71 and 1.85, respectively, which are far greater than the anomaly values of the single preceding winter pNAM events (− 0.27 and 0) and single spring nTNA SSTA events (− 0.74 and 0.19). The above analysis indicates that the MHEA tends to experience a warm spring, and the extreme cold events occur far less and are weaker than normal when both the preceding winter pNAM and spring nTNA SSTA occur, which further indicates that there is a strong synergistic effect from the preceding winter pNAM and spring nTNA SSTA with respect to spring extreme cold events in the MHEA.

To further compare the spatial characteristics of the spring extreme cold anomalies from different events, Fig. 4 shows the composite spatial distributions of spring TN10p and TNn anomalies from the joint events pNAM ⊕ nTNA, single preceding winter pNAM events, and single spring nTNA SSTA events. Compared with the single preceding winter pNAM events and single spring nTNA SSTA events, the composite maps of extreme spring temperature indices for the joint events pNAM ⊕ nTNA have a large same-sign area over the MHEA, extending from 70°E to the east side of the MHEA continent, with the greatest anomaly in the central area of the MHEA (Fig. 4). Based on Li et al. (2019a), the synergistic effect of the preceding winter pNAM and spring nTNA SSTA on the spring extreme cold events is significant in this area, especially in the region that is the most closely correlated with the NAM. The spatial distribution shown in Fig. 4 is consistent with Fig. 3, further supporting the strong synergistic effect of the preceding winter pNAM and spring nTNA SSTA on weakening and decreasing the spring extreme cold events in the MHEA. As the interannual variations and spatial distributions of the various extreme temperature indices anomalies across the MHEA are similar, we will focus on TN10p in the rest of this paper.

To investigate the mechanism associated with the synergistic influence of the two factors on the spring extreme cold events in the MHEA, Fig. 5a shows the correlation map between the spring TN10p in the MHEA and the spring 500-hPa geopotential height. There is an area of significantly negative correlation on the east side of the Eurasian continent and over the adjacent Okhotsk Ocean. This implies that the spring atmospheric circulation anomaly in this area is vital to the variation of the spring extreme cold events in the MHEA. When a strong anomalous anticyclone appears in this area, the extreme cold events decrease and weaken in the MHEA. Thus, we use the spring area-averaged 500-hPa geopotential height anomaly across the domain 45°–70° N, 90°–150° E as the spring MHEA anomalous anticyclone index to quantify the anomalous atmospheric circulation.

Figure 5b shows the time series of the spring MHEA anomalous anticyclone index and TN10p in spring. The spring MHEA anomalous anticyclone index is highly correlated with TN10p, with a correlation coefficient of − 0.75, far exceeding the 99% confidence level. This indicates that the spring MHEA anomalous anticyclone may lead to a decrease and weakening of the spring extreme cold events in the MHEA.

In the large-scale atmospheric circulation, changes in air temperature can be caused by horizontal temperature advection, the vertical motion of air, and diabatic heating (e.g., longwave and shortwave radiation). The atmospheric thickness mentioned in Sect. 2 is a key factor that can be used to investigate changes in air temperature caused by changes in the atmospheric circulation (Li et al. 2021). From the perturbation thermodynamic equation, horizontal temperature advection can be written as $-\left(u'\frac{\partial \overline{T}}{\partial x}+v'\frac{\partial \overline{T}}{\partial y}+\overline{u}\frac{\partial T'}{\partial x}+\overline{v}\frac{\partial T'}{\partial y}\right)$, and the temperature change caused by the vertical motion of air is represented as $-\left(\gamma_d-\gamma\right)w$. To investigate how the spring MHEA anomalous anticyclone influences the spring extreme cold events in the MHEA, Fig. 5c shows the correlations of the spring area-averaged horizontal temperature

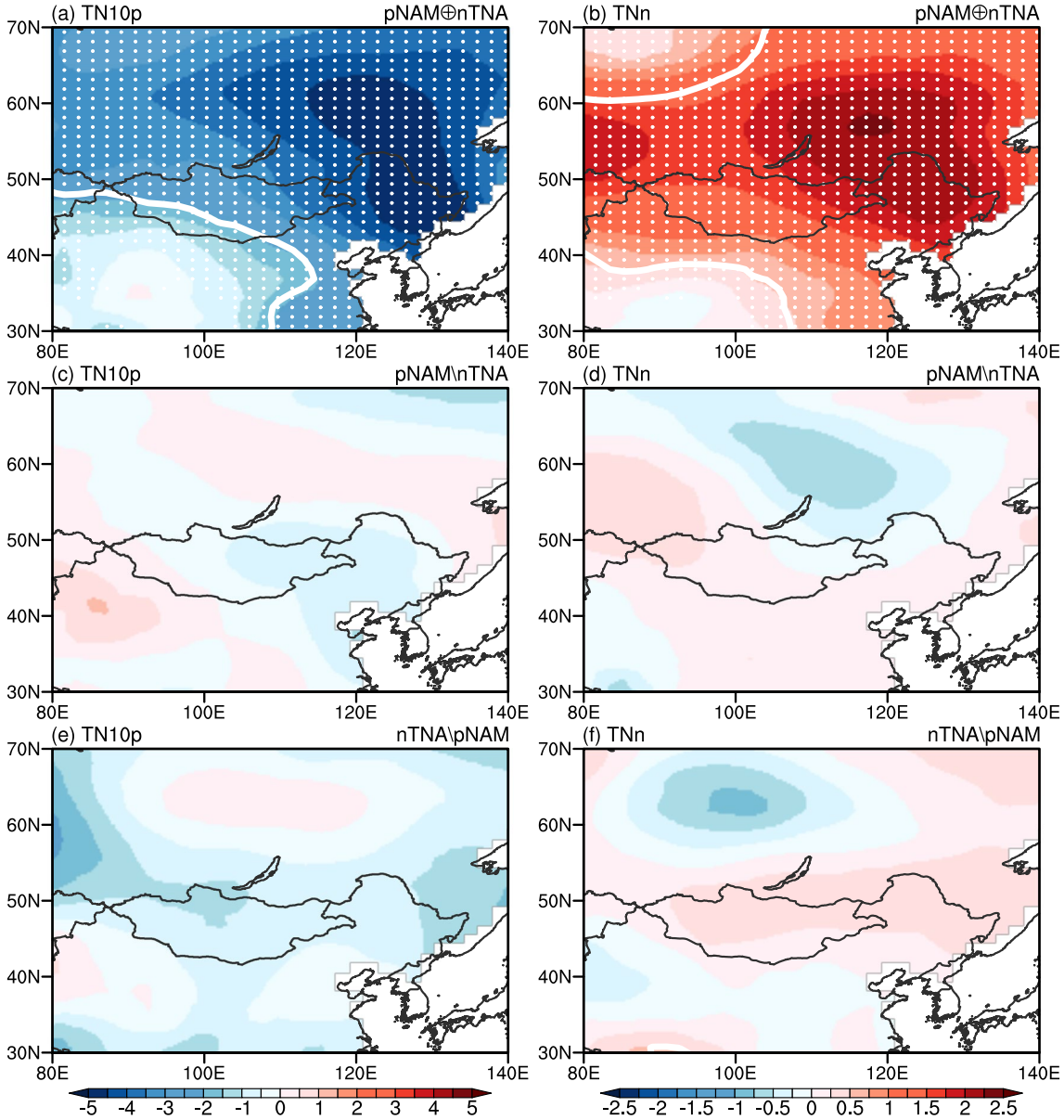

Fig. 4 Composite maps of spring extreme temperature indices for different events. **a** TN10p (%) for the joint events of preceding winter pNAM and spring nTNA SSTA (pNAM ⊕ nTNA). The white dotted areas indicate the synergistic effect of preceding winter pNAM and spring nTNA SSTA. The white contour lines indicate significant values at the 95% confidence level based on the Student *t* test. **b** As in **a** but for spring TNn (°C). **c** As in **a**, but for the single preceding winter pNAM events. **d** As in **b**, but for the single preceding winter pNAM events. **e** As in **a**, but for the single spring nTNA SSTA events. **f** As in **b**, but for the single spring nTNA SSTA events

advection, temperature change caused by the vertical motion of air, 500–1000 hPa atmospheric thickness, and the difference between the net shortwave and longwave radiation flux in the MHEA with the spring MHEA anomalous anticyclone index. The correlation coefficient between the spring MHEA anomalous anticyclone index and area-averaged horizontal temperature advection in the MHEA is 0.58 (significant at the 99% confidence level), indicating that the stronger the spring MHEA anomalous anticyclone is, the greater the spring horizontal warm advection in the MHEA will be. As shown in Fig. 5a, the MHEA continent is located in the western part of the spring MHEA anomalous anticyclone, which is featured with southerly winds. The southerly winds deliver warm air from the lower latitudes to the MHEA, which favors the increase in air temperature in the MHEA. In addition, the correlation coefficient between the spring MHEA anomalous anticyclone and temperature increase caused by the vertical motion of air in the MHEA is 0.40, which is also significant at the 99% confidence level. This reflects a scenario in which the spring MHEA anomalous anticyclone

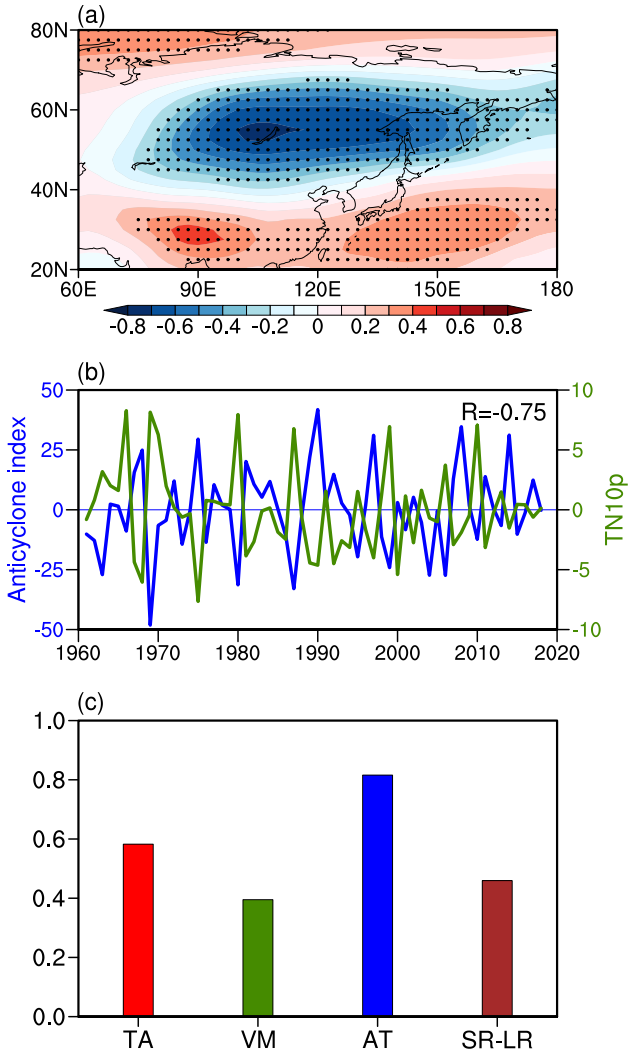

Fig. 5 **a** The correlation map between the spring TN10p in the MHEA and spring 500-hPa geopotential height. Dotted areas indicate significant values at the 95% confidence level based on the Student *t* test. **b** Time series of the spring MHEA anomalous anticyclone index and TN10p in spring. **c** Correlations of the spring area-averaged horizontal temperature advection (TA), temperature change caused by the vertical motion (VM), 500–1000 hPa atmosphere thickness (AT), difference between the net shortwave and longwave radiation flux (SR–LR) in the MHEA with the spring MHEA anomalous anticyclone index

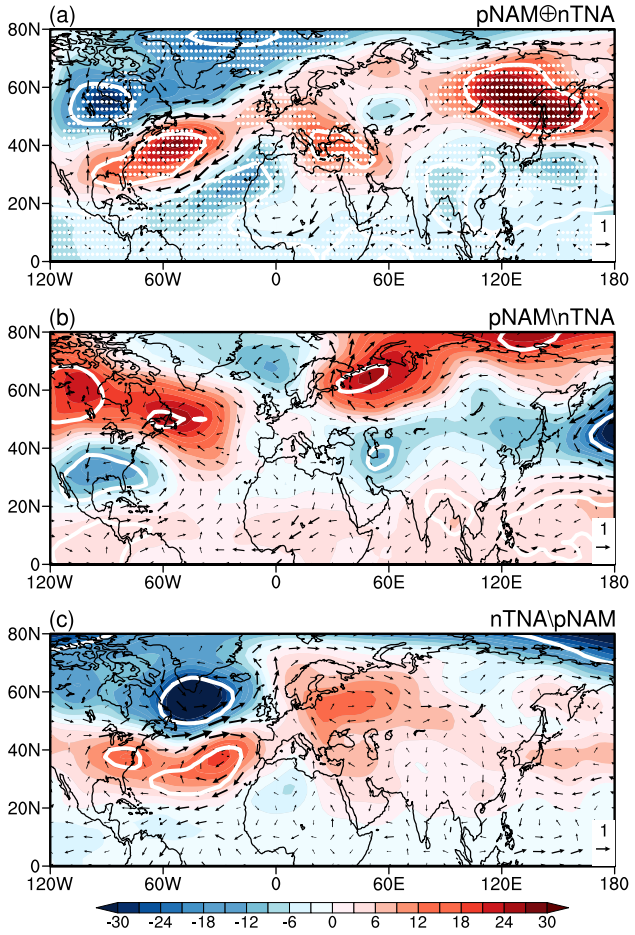

Fig. 6 Composite maps of the spring 500-hPa geopotential height (gpm; shaded) and 850-hPa winds (m s^{-1}; vectors) at for **a** the joint events of preceding winter pNAM and spring nTNA (pNAM ⊕ nTNA), **b** single preceding winter pNAM events and **c** single spring nTNA SSTA events. The white dotted areas in **a** indicate the synergistic effect of preceding winter pNAM and spring nTNA SSTA. The white contour lines indicate significant values at the 95% confidence level based on the Student *t* test

generates the sinking motion over the MHEA, which in turn leads to an increase in the air temperature. There is a high positive correlation coefficient (0.82) between the spring MHEA anomalous anticyclone index and the atmospheric thickness in the MHEA, and this implies that the atmospheric thickness anomaly is a reflection of the upper-level geopotential height anomaly. The anomalous anticyclone can weaken the spring extreme cold events in the MHEA by increasing the atmospheric thickness in the MHEA, because the atmospheric thickness anomaly is proportional to the change of the mean air temperature of the atmospheric layer (Li et al. 2021). In addition, the correlation coefficient between the spring MHEA anomalous anticyclone and the net radiation flux is 0.41, which is also above the 99% confidence level. The sinking motion brought about by the spring MHEA anomalous anticyclone restricts cloud formation in the MHEA. The decrease in cloud cover leads to an increase in net radiation received by the surface, causing the decrease and weakening of the spring extreme cold events in the MHEA.

Figure 6 shows the composite maps of the spring 500-hPa geopotential height and 850-hPa wind anomalies for the three different types of event. In the joint events pNAM ⊕ nTNA, there are strong positive geopotential height anomalies in the MHEA, mainly around the east side of the Eurasian continent and over the adjacent Okhotsk Ocean,

extending from 90° E to around 160° E (Fig. 6a). However, for the single preceding winter pNAM events, there is no obvious spring MHEA anomalous anticyclone over East Asia, but a weak positive geopotential height anomaly in the north of the MHEA (Fig. 6b). For the single spring nTNA SSTA events, a considerably weak anomalous anticyclone appears over the MHEA. Compared with the joint events pNAM ⊕ nTNA, the area of the anomalous anticyclone associated with the single spring nTNA SSTA events is smaller and most of the anomalous anticyclone is around the Okhotsk Ocean instead of over the east of the mid-high latitudes Eurasian continent. This implies that the anomalous anticyclone can impact only a smaller area with the reduced strength of influence (Fig. 6c). In addition, as shown in the time series of the spring MHEA anomalous anticyclone index in Fig. 5a, the spring MHEA anomalous anticyclone index for the joint events pNAM ⊕ nTNA is much larger than for the two single events, and 6 out of the 7 joint events pNAM ⊕ nTNA have positive anomalies (the only negative anomaly is relatively weak), which is similar to the extreme temperature indices.

The above analysis indicates that the preceding winter pNAM and spring nTNA SSTA have a strong synergistic effect on the spring anomalous anticyclone over the MHEA, which means that the cooccurrence of the preceding winter pNAM and spring nTNA SSTA lead to the strong spring anomalous anticyclone over the MHEA. This strong spring anomalous anticyclone over the MHEA gives rise to a significant increase in surface air temperature over the MHEA through the processes in Fig. 5c. Thus, it is unfavorable for the spring extreme cold events in the MHEA, and the MHEA is likely to experience a warm spring. This means that taking both the preceding winter pNAM and spring nTNA SSTA into consideration while predicting and studying the spring extreme cold events in the MHEA is of vital importance.

4 Mechanism of the synergistic effect

Previous studies found that the East Asian surface air temperature during spring is closely correlated with the spring EASCE (Yin et al. 2013; Ye and Lau 2019; Zhou et al. 2021). The NAM in winter is closely related to the EASCE through the temperature anomalies produced by the NAM, and the EASCE anomalies that store the NAM signal can persist for a long time (Bamzai 2003; Robock et al. 2003; Saito and Cohen 2003; Saito et al. 2004). Therefore, the preceding winter pNAM can reduce the EASCE, and the EASCE plays the role of a snow cover bridge. Figure 7a shows the time series of the spring EASCE anomalies and spring MHEA anomalous anticyclone index. The variations of the spring MHEA anomalous anticyclone correspond well with variations in the spring EASCE, with a correlation coefficient of − 0.49, which is significant at the 99% confidence level. Figure 7b shows the correlation map between the 500-hPa geopotential height and EASCE anomalies in spring. There is a significant negative correlation coefficient on the MHEA continent and over the adjacent Okhotsk Ocean. In addition, this large area with the negative correlation is significant at the 95% confidence level, indicating the strong connection between the spring EASCE and atmospheric circulation over the MHEA. Figure 7d shows the composite map of the spring 500-hPa geopotential height and wind anomalies for the joint events pNAM ⊕ nTNA. The highly correlated area in Fig. 7b is similar to the area of high positive geopotential height anomalies in Fig. 7d. This further indicates that the spring anomalous anticyclone is closely related to the spring EASCE, and the spring EASCE affects the spring extreme cold events in the MHEA through the atmospheric circulation over the MHEA.

Figure 7c shows the spring EASCE anomalies for the three types of events. There is a strong decrease in the spring EASCE in the joint events pNAM ⊕ nTNA, which can lead to the strong spring anomalous anticyclone over the MHEA. However, for the two types of single event, the decrease in the spring EASCE is far weaker than that for the joint events pNAM ⊕ nTNA. In addition, the time series of spring EASCE anomalies (Fig. 7a) shows that the amplitudes of the joint events pNAM ⊕ nTNA are greater than those of the single events. It is also worth noting that 6 of the 7 pNAM ⊕ nTNA events have positive EASCE anomalies (the only negative anomaly is also relatively weak), which matches the extreme spring temperature indices and the MHEA spring anomalous anticyclone index, and this means that there is a higher same-sign rate in the joint events pNAM ⊕ nTNA than that in the single spring nTNA SSTA events or single preceding winter pNAM events. The spatial patterns of snow cover anomaly in the three types of events are shown in Fig. 8. In the joint events pNAM ⊕ nTNA, the strong negative anomaly of snow cover covers a large area in the MHEA, and the preceding winter pNAM and spring nTNA SSTA exhibit an obvious synergistic effect over the MHEA (Fig. 8a). However, as for the single preceding winter pNAM events (Fig. 8b) and the single spring nTNA SSTA events (Fig. 8c), there are few small areas showing significant anomaly of snow cover in the MHEA.

The above analysis shows that the preceding winter pNAM and spring nTNA SSTA act synergistically to reduce the spring EASCE. The EASCE anomalies for the joint events pNAM ⊕ nTNA and single preceding winter pNAM events are roughly equal in the preceding winter. However, the difference of the EASCE anomalies for the two events gradually becomes larger after the preceding winter (not shown). The large reduction of EASCE in the joint events pNAM ⊕ nTNA leads to the strong spring

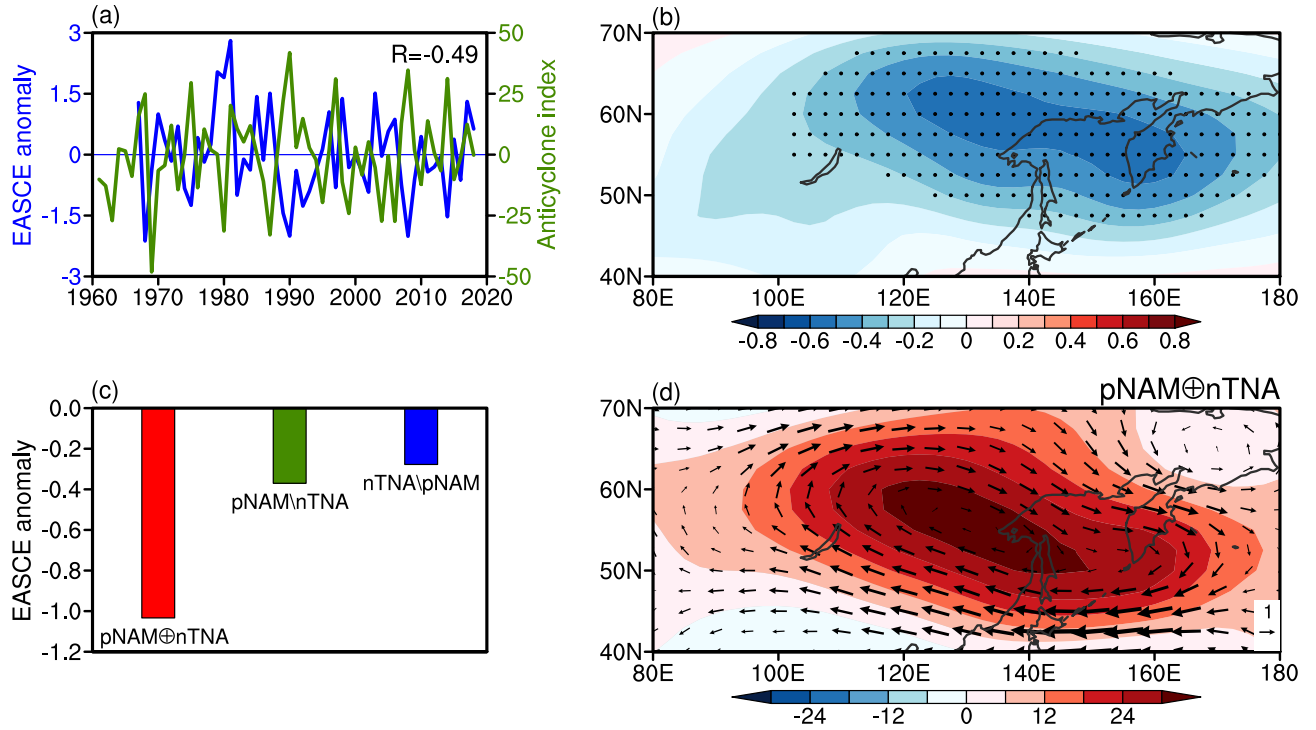

Fig. 7 **a** Time series of the spring EASCE anomalies (blue line, unit: 10^6 km^2) and spring MHEA anomalous anticyclone index (green line). **b** Correlation between the geopotential height (gpm) at 500-hPa and EASCE anomalies (10^6 km^2) in spring. Dotted areas indicate the significant values at the 95% confidence level based on the Student *t* test. **c** The spring area-averaged EASCE anomalies (10^6 km^2) for the joint events pNAM ⊕ nTNA (red), single preceding winter pNAM events (green) and single spring nTNA SSTA events (blue) in spring. **d** The composite map of spring 500-hPa geopotential height (gpm; shaded) and 850-hPa winds (m s^{-1}; vectors) for the joint events pNAM ⊕ nTNA

anomalous anticyclone over the MHEA around the east side of the Eurasian continent via the snow-hydrological effect, which suggests that the negative snow cover anomaly can lead to the anticyclone over the MHEA through the reduced soil moisture (Matsumura et al. 2010, 2015; Matsumura and Yamazaki 2012; Yin et al. 2013; Liu et al. 2020). Thus, the preceding winter pNAM and spring nTNA exert their synergistic effect on the MHEA anomalous anticyclone via the snow cover bridge. Through the process of temperature advection, the vertical motion of air, atmospheric thickness, and radiation in the MHEA, the two factors exert their synergistic effect on spring extreme cold events in the MHEA, which are greatly suppressed in the joint events pNAM ⊕ nTNA.

As there is an evident synergistic effect of the preceding winter pNAM and spring nTNA SSTA on the spring MHEA anomalous anticyclone, we will now consider how the spring nTNA SSTA acts synergistically with the preceding winter pNAM and further influences the air temperature in the MHEA. Figure 10a shows the composite map of the spring 500-hPa geopotential height anomalies for all spring nTNA SSTA events. The atmospheric circulation beyond the Atlantic displays a dipole mode from the polar to the extratropical area, which is an atmospheric circulation pattern similar to a positive North Atlantic Oscillation (NAO). The NAO can be seen as a branch of the NAM in the Atlantic, and the circumglobal atmospheric circulation displays evident annular mode characteristics (Fig. 9a).

This result is consistent with a previous study that demonstrate that the spring TNA SSTA can force the NAO-like atmospheric response through the wind–evaporation–sea surface temperature (WES) feedback (Wu et al. 2007). That is, when the spring TNA SST drops, the atmospheric circulation favors the formation of the spring pNAM, and the spring pNAM will store the signal of the spring nTNA SSTA in the spring EASCE, which can release the signal into the atmosphere in the MHEA. In this process, the spring nTNA SSTA sends its signal to the atmospheric circulation in the MHEA via the atmospheric bridge of an NAO-like atmospheric response and the snow cover bridge of the EASCE. The spring nTNA-induced pNAM can be seen as the persistence of the preceding winter pNAM; i.e., the pNAM can persist from the preceding winter to spring in the joint events pNAM ⊕ nTNA.

The above analysis implies that the spring nTNA SSTA may amplify the signal of the preceding winter pNAM by

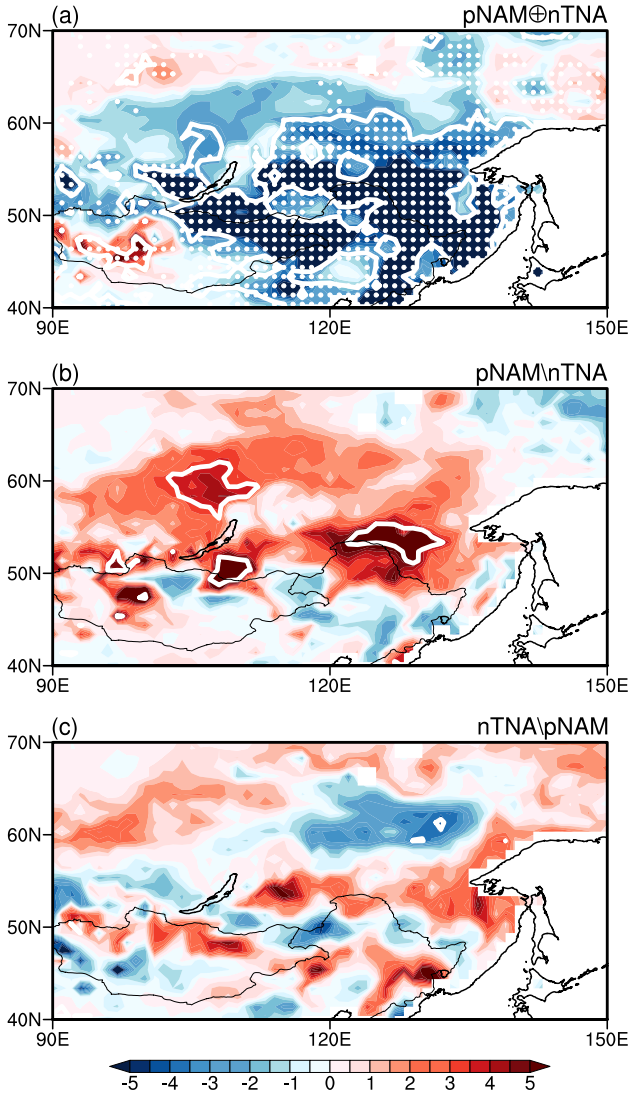

Fig. 8 Composite maps of the spring snow cover anomaly (%) for **a** the joint events of preceding winter pNAM and spring nTNA (pNAM ⊕ nTNA), **b** single preceding winter pNAM events and **c** single spring nTNA SSTA events. The white dotted areas in **a** indicate the synergistic effect of preceding winter pNAM and spring nTNA SSTA. The white contour lines indicate significant values at the 95% confidence level based on the Student *t* test

inducing the spring pNAM, and the spring pNAM is a key factor in the atmospheric bridge linking the spring nTNA SSTA to the spring EASCE. To reveal how important the persistence of the pNAM is to the variability of the spring EASCE, Fig. 9b shows the spring EASCE anomalies for the different NAM combinations from the preceding winter and following spring. We divided the pNAM into three categories; i.e., only the preceding winter pNAM occurs, only the spring pNAM occurs, and cooccurrence of the preceding winter pNAM and spring pNAM. As shown in Fig. 9b, all three pNAM scenarios can induce a reduction in the spring EASCE. However, with respect to the degree of reduction, the three scenarios show different characteristics. Compared with the preceding winter-only and spring-only pNAM events, there is a much stronger negative anomaly of the spring EASCE if the preceding winter and spring pNAM both occur, and the negative spring EASCE anomaly value is − 0.69. This indicates that the persistence of the pNAM from the preceding winter to spring leads to a greater reduction in the spring EASCE. This result further demonstrates why joint events pNAM ⊕ nTNA generate a larger spring EASCE anomaly than the two single events.

Other than sending its signal to the atmospheric circulation in the MHEA through the atmospheric bridge of the spring pNAM and the snow cover bridge of the decreased EASCE in turn, there may be another way for the spring nTNA SSTA to affect the atmospheric circulation in the MHEA. To investigate the dynamic mechanism that allows the spring nTNA SSTA to affect the atmospheric circulation in the MHEA, we applied the horizontal wave activity flux proposed by Takaya and Nakamura (2001). As shown in Fig. 10a, the spring nTNA can excite the easterly propagating Rossby wave, and the Rossby wave energy can propagate northeastwards into the MHEA. The Rossby wave energy over the eastern side of the Eurasian continent can excite the spring MHEA anomalous anticyclone and further impact on the spring extreme cold events in the MHEA. Thus, the easterly propagating Rossby wave plays the role of another atmospheric bridge linking the spring nTNA SSTA to the spring MHEA anomalous anticyclone.

To further confirm that the eastward Rossby wave is another such atmospheric bridge, we use the approach of Rossby wave ray tracing in a horizontally nonuniform background flow developed by Li and Li (2012), Li et al. (2015, 2019b, 2021), and Zhao et al. (2015, 2019). Figure 10b shows the stationary Rossby wave trajectories in the horizontally nonuniform flow for the spring nTNA SSTA events at 500-hPa. The starting region is set in the TNA, there are easterly propagating Rossby wave rays along the Eurasian continent, and the Rossby wave rays concentrate over the eastern side of the MHEA continent. The stationary Rossby wave trajectories indicate that the concentrated Rossby wave energy favors the formation of an anomalous anticyclone over the MHEA, which is consistent with the wave activity flux in Fig. 10a. The Rossby wave induced by the spring nTNA SSTA acts jointly with the diminished spring EASCE, leading to the strong MHEA anomalous anticyclone, and then the decrease and weakening of the spring extreme cold events in the MHEA. The above results show that the spring nTNA SSTA has a synergistic impact on the spring MHEA anomalous anticyclone jointly with the preceding winter pNAM via the snow cover bridge of the spring decreased EASCE and the atmospheric bridge of the easterly propagating Rossby wave.

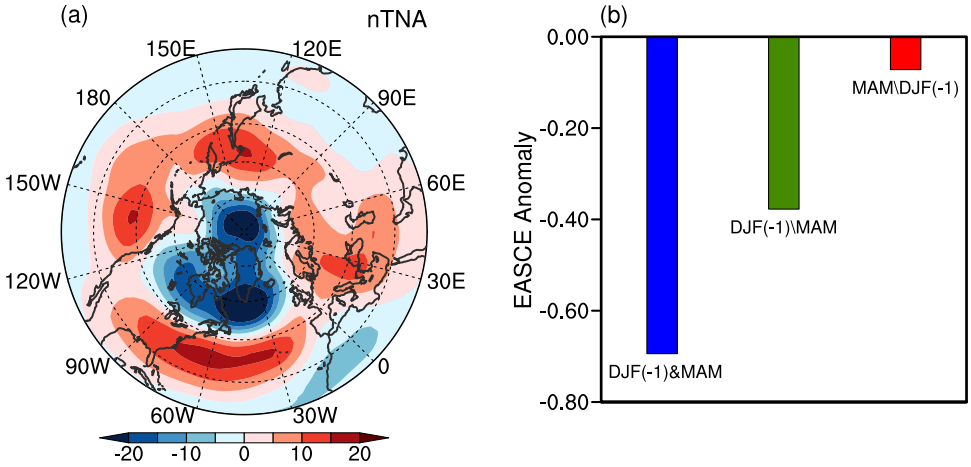

Fig. 9 **a** The composite map of spring 500-hPa geopotential height (gmp) for all the spring nTNA SSTA events. **b** The spring EASCE anomalies (10^6 km^2) for different NAM combinations. The red, green and blue bars represent the spring-only pNAM events, preceding winter-only pNAM events and cooccurrence of the spring and preceding winter pNAM respectively

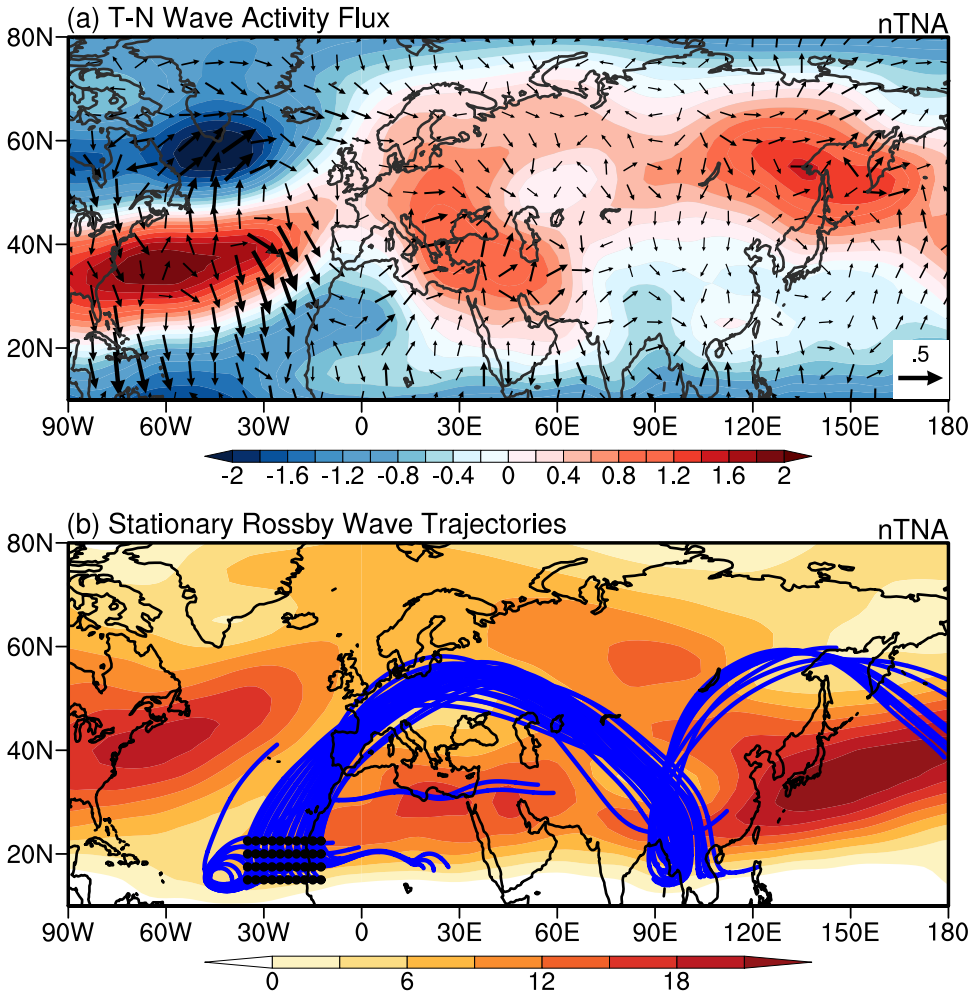

Fig. 10 **a** The composite map of spring 500-hPa T-N wave activity flux (m^2 s^{-2}; vectors) and anomalous QG stream function (m^2 s^{-1}; shaded) for all the spring nTNA SSTA events. **b** Spring stationary Rossby wave trajectories in the horizontally nonuniform flow (blue curves) with zonal wavenumber $k=4$ for all the spring nTNA SSTA events. The black dots denote the Rossby wave source. The shaded area is the climatological mean 500-hPa zonal wind (m s^{-1}). The Rossby wave ray tracing is calculated by adopting the approach by Li and Li (2012), Li et al. (2015, 2019b, 2021) and Zhao et al. (2015)

The LBM is used to confirm the heating effect of snow cover anomaly and nTNA SSTA on the atmospheric circulation. Three experiments are carried in the LBM. In the first experiment (EXP1), to simulate the heating effect of snow cover anomaly, the heating source is set in the domain 40°–60° N, 100°–140° E, where the snow cover significantly decreases in the joint events (Fig. 8a). In the second experiment (EXP2), the heating sink is set in the domain 0°–20° N, 20°–80° W, which is the same as the TNA SST region. The third experiment (EXP3) is the combination of the EXP1

and EXP2, including the heating source of EXP1 and heating sink of the EXP2. Figure 11 shows the steady 500 hPa geopotential height response in the three experiments. As shown in Fig. 11a, the heating source of EXP1 can induce the anomalous anticyclone over MHEA and its adjacent Okhotsk. This is consistent with the previous studies demonstrating that the decreased snow cover can produce the heating effect and thereby induce the anomalous anticyclone via the snow-hydrological effect (Matsumura et al. 2010, 2015; Matsumura and Yamazaki 2012; Yin et al. 2013; Liu et al. 2020). Besides, as shown in Fig. 11b, the atmospheric response to the TNA heating sink shows the NAO-like pattern over the Atlantic and relatively weak positive geopotential height anomaly over MHEA, which is consistent with the observational results. In the EXP3, the combination of the two heating forcings indicates a synergistic effect on the MHEA anomalous anticyclone, which implies that the MHEA anomalous anticyclone is strengthened by the two heating forcings, and confirms the effect of snow cover anomaly and TNA SSTA on the MHEA anomalous anticyclone (Fig. 11c). The LBM results confirm the effect of the EASCE and TNA SST on the atmospheric circulation, which can further influence the spring extreme cold temperature events in the MHEA.

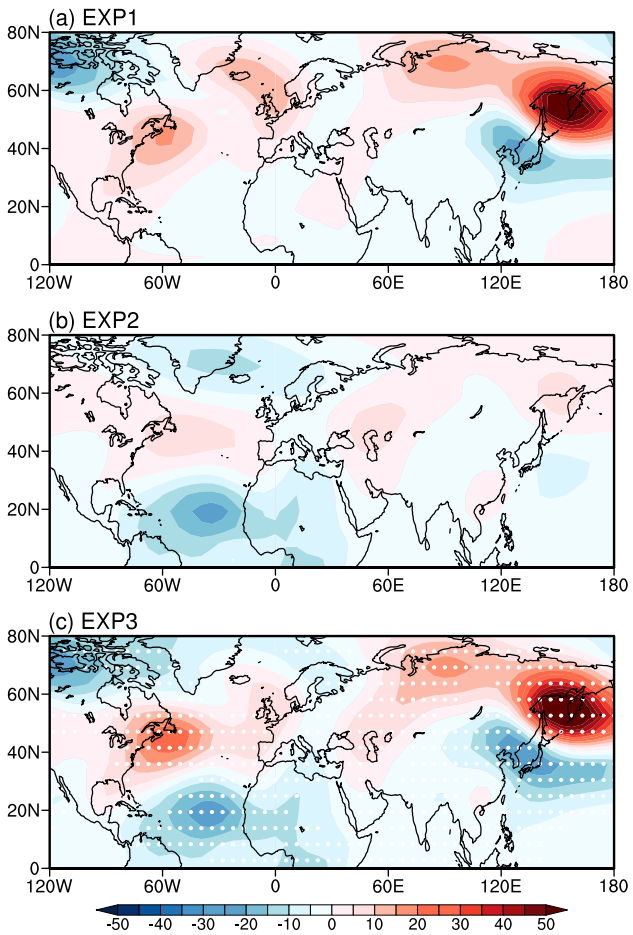

Fig. 11 Steady 500 hPa geopotential height response (gpm) to **a** the snow cover heating source, **b** TNA heating sink and **c** combination of snow cover heating source and TNA heating sink. The white dotted areas in **c** indicate the synergistic effect of the EASCE heating source and TNA heating sink

5 Summary and discussion

In this paper, we have demonstrated that the preceding winter pNAM and the spring nTNA SSTA have a synergistic effect that leads to a significant decrease in extreme cold events in the MHEA. Both the single preceding winter pNAM and single spring nTNA SSTA can slightly decrease and weaken the extreme cold events in the MHEA. However, when both factors occur, the reduction in intensity of the extreme cold events is much greater than that caused by either factor alone, and the probability of a weakened extreme cold event is far greater than that associated with a single factor event. It is worth noting that the region affected is not confined to northeast China, but covers a much larger area of the MHEA.

Figure 12 summarizes the process associated with the synergistic effect of the preceding winter pNAM and the spring nTNA SSTA on the extreme cold events in the MHEA. The preceding winter pNAM can store its signal in the EASCE, which diminishes the simultaneous EASCE. Owing to the persistence of the snow cover, the negative EASCE anomaly can persist into the spring of the following year (Bamzai 2003; Robock et al. 2003; Saito and Cohen 2003; Saito et al. 2004). This process is seen as the snow cover bridge sending the signal from the preceding winter pNAM to the atmospheric circulation over the MHEA. In spring, the occurrence of the spring nTNA SSTA forces a positive NAO-like atmospheric response, leading to the formation of the anomalous high (low) pressure over the subtropical Atlantic (subpolar area of the Atlantic; Wu et al. 2007). As the NAO can be seen as a branch of the NAM over the Atlantic region, the spring TNA SST cooling could result in the spring pNAM. Then, the spring pNAM induced by the spring nTNA SSTA can further reduce the simultaneous EASCE.

By comparing the response of the spring EASCE anomalies with different NAM phase combinations in the preceding winter and spring, we find that the spring EASCE exhibits the greatest negative anomaly when the pNAM persists from the preceding winter to the following spring. As a result, by inducing the pNAM atmospheric response in spring, the spring nTNA SSTA and the preceding winter pNAM exert a synergistic effect that causes the great reduction in the spring EASCE. The reduction of EASCE can induce the anomalous anticyclone over the MHEA via

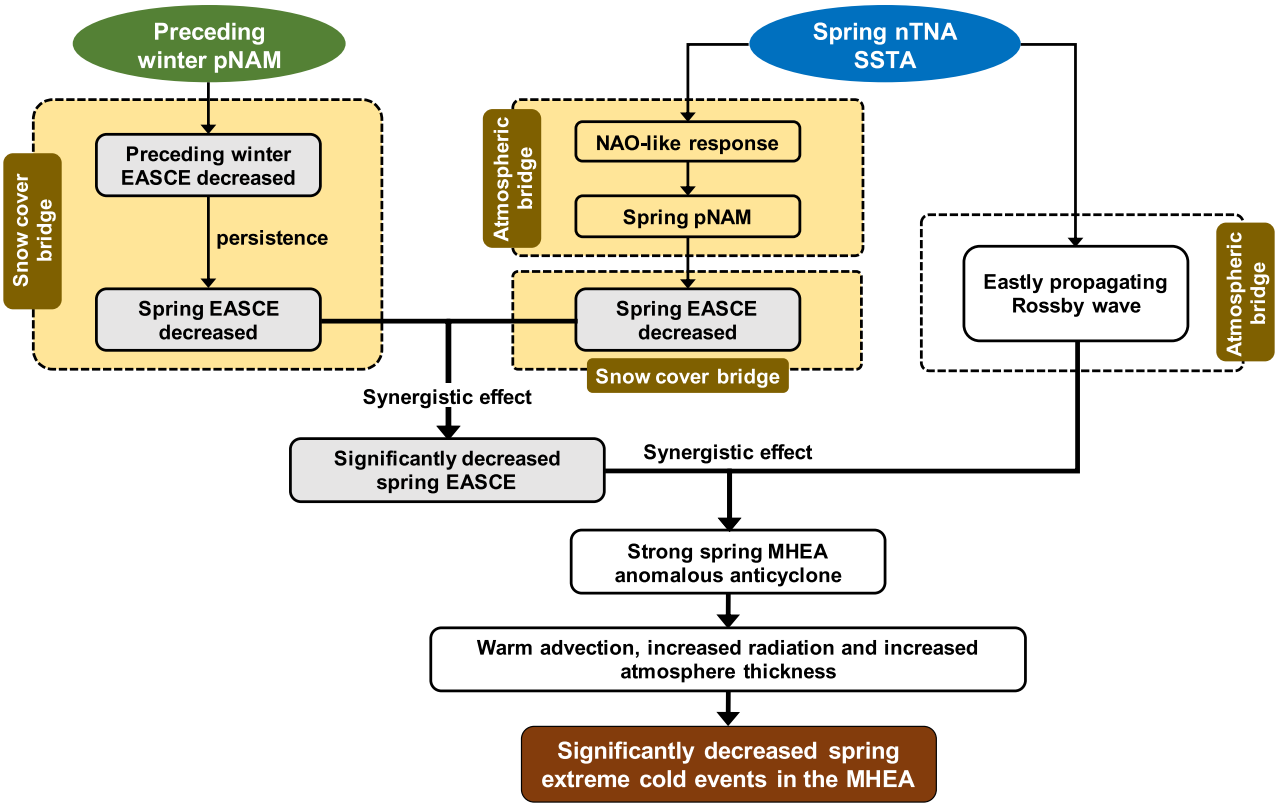

Fig. 12 The schematic diagram showing the synergistic effect of the preceding winter pNAM and spring nTNA SSTA on the spring extreme cold events in the MHEA. The yellow shaded parts indicate that there are previous studies in the processes

the snow-hydrological effect (Matsumura et al. 2010, 2015; Matsumura and Yamazaki 2012; Yin et al. 2013; Liu et al. 2020). The above processes show that the positive spring NAO-like atmospheric response induced by the spring nTNA SSTA acts as the atmospheric bridge, and the spring EASCE acts as the snow cover bridge. These two bridges together send the signal of the spring nTNA SSTA to the atmospheric circulation over the MHEA.

As a result of the significant decrease in the spring EASCE (i.e., the snow cover bridge), the two factors also have an evident synergistic effect on the spring MHEA anomalous anticyclone, which is strongest in the joint events pNAM ⊕ nTNA. We found that the strength of the spring MHEA anomalous anticyclone is closely related to horizontal temperature advection, the temperature increase caused by the vertical motion of air, atmospheric thickness, and net shortwave and longwave radiation in the MHEA. The anomalous southerly winds on the western side of the spring MHEA anomalous anticyclone cause warm advection that brings warm air from the south and leads to the increase in air temperature and the weakening of the extreme cold events in spring in the MHEA.

In addition, according to the perturbation hypsometric equation, the increased atmospheric thickness can lead to an increase in the mean air temperature of the atmospheric layer. Furthermore, the anomalous high pressure over the MHEA can become a barrier that is able to hinder the southern movement of the cold air from the polar area. Therefore, the above process further decreases and weakens the spring extreme cold events in the MHEA.

In addition to the above atmospheric processes, the anomalous high pressure can also change the net radiation in the MHEA. The sinking motion caused by the anomalous high pressure hinders cloud formation, and thereby increases net radiation received at the surface, and further leads to warmer air temperatures, and less and weaker spring extreme cold events than normal in the MHEA.

In addition to influencing the atmospheric circulation over the MHEA through the snow cover bridge of the spring EASCE, the spring nTNA SSTA has an additional impact on the atmospheric circulation over the MHEA via the atmospheric bridge of the Rossby wave train. We have revealed that the Rossby wave energy over the Eurasian continent favors the propagation of the Rossby wave downstream when the spring nTNA SSTA occurs, which can affect the 500-hPa geopotential height over the MHEA and favor the formation of the spring MHEA anomalous anticyclone. This atmospheric process further increases the air temperature

and weakens the spring extreme cold events. In the end, the MHEA may experience a warmer spring.

In this paper, we have analyzed the synergistic effect of the preceding winter pNAM and spring nTNA SSTA on the interannual variability of the spring extreme cold events in the MHEA. However, one extreme cold case in East Asia may be influenced by some weather processes, such as the cold vortex. Thus, the whole process of one extreme temperature case needs the further detailed analysis. Besides, it can be seen from Fig. 2 that SSTs over some places are also significantly correlated with the extreme cold temperature events in the MHEA. This indicates that SSTs in these places might have synergistic effects with other factors on influencing the spring extreme cold events over MHEA, and the synergistic effects need more further studies. Note that we analyzed only two influencing factors over the interannual timescale in this study because of the length of the available dataset, but extreme temperature can be influenced by more than these two factors. If we take multiple factors into consideration, observational data covering a much longer period will be required to obtain an adequate sample size. Consequently, a longer observational dataset and comprehensive consideration of the synergistic effects of multiple factors will be required in a future study.

Acknowledgements Hao Wang and Yina Diao contributed equally to this work. We wish to thank all the data providers, and the two anonymous reviewers for the valuable suggestions and comments. This work is supported by the National Natural Science Foundation of China (NSFC) Project (41790474), Shandong Natural Science Foundation Project (ZR2019ZD12), and Fundamental Research Funds for the Central Universities (201962009). Dr. Fei Zheng is surported by China Association for Science and Technology Working Group for UN Environment Consultation. We are grateful to Center for High Performance Computing and System Simulation, Pilot National Laboratory for Marine Science and Technology (Qingdao) for providing computing resource.

References

Bamzai A (2003) Relationship between snow cover variability and Arctic Oscillation index on a hierarchy of time scales. Int J Climatol 23(2):131–142

Chen TC, Yen MC, Huang WR, Gallus WA (2002) An East Asian cold surge: case study. Mon Weather Rev 130(9):2271–2290

Chen TC, Huang WR, Yoon J (2004) Interannual variation of the East Asian cold surge activity. J Clim 17(2):401–413

Chen S, Wu R, Liu Y (2016) Dominant modes of interannual variability in Eurasian surface air temperature during boreal spring. J Clim 29:1109–1125

Cheung HN, Zhou W, Mok HY, Wu MC (2012) Relationship between ural-Siberian blocking and the East Asian winter monsoon in relation to the Arctic Oscillation and the El Nino–Southern Oscillation. J Clim 25(12):4242–4257

Dunn RJH, Alexander LV, Donat MG et al (2020) Development of an updated global land in situ-based data set of temperature and precipitation extremes: HadEX3. J Geophys Res Atmos 125(16):e2019JD032263

Easterling DR (2000) Climate extremes: observations, modeling, and impacts. Science 289(5487):2068–2074

Gong DY, Ho CH (2002) The Siberian high and climate change over middle to high latitudeAsia. Theor Appl Climatol 72(1):1–9

Gong DY, Yang J, Kim SJ, Gao Y, Guo D, Zhou T, Hu M (2011) Spring Arctic Oscillation-East Asian summer monsoon connection through circulation changes over the western North Pacific. Clim Dyn 37:2199–2216

Hersbach H, Bell B, Berrisford P, Hirahara S, Horányi A, Muñoz-Sabater J et al (2020) The ERA5 global reanalysis. Q J R Meteorol Soc 146:1999–2049

Hoskins BJ, Karoly DJ (1981) The steady linear response of a spherical atmosphere to thermal and orographic forcing. J Atmos Sci 38:1179–1196

Huang J, Yu H, Guan X, Wang G, Guo R (2016) Accelerated dryland expansion under climate change. Nat Clim Change 6:166–171

Jeong J-H, Kim B-M, Ho C-H, Noh Y-H (2008) Systematic variation in wintertime precipitation in East Asia by MJO-induced extratropical vertical motion. J Clim 21(4):788–801

Kalnay E, Kanamitsu M, Kistler R et al (1996) The NCEP/NCAR 40-year reanalysis project. Bull Am Meteorol Soc 77(3):437–471

Karoly DJ (1983) Rossby wave propagation in a barotropic atmosphere. Dyn Atmos Oceans 7:111–125

Li SL (2004) Impact of northwest Atlantic SST anomalies on the circulation over the Ural Mountains during early winter. J Meteorol Soc Jpn 82:971–988

Li Y, Li JP (2012) Propagation of planetary waves in the horizontal non-uniform basic flow (in Chinese). Chin J Geophys 55(2):361–371

Li L, Nathan TR (1997) Effects of low-frequency tropical forcing on intraseasonal tropical-extratropical interactions. J Atmos Sci 54:332–346

Li JP, Ruan CQ (2018) The North Atlantic-Eurasian teleconnection in summer and its effects on Eurasian climates. Environ Res Lett 13:024007

Li JP, Wang JXL (2003) A modified zonal index and its physical sense. Geophys Res Lett 30:1632

Li JP, Wu ZW (2012) Importance of autumn Arctic sea ice to northern winter snowfall. Proc Natl Acad Sci 109:E1898

Li Y, Li JP, Jin FF, Zhao S (2015) Interhemispheric propagation of stationary Rossby waves in the horizontally nonuniform background flow. J Atmos Sci 72(8):3233–3256

Li JP, Zheng F, Sun C, Feng J, Wang J (2019a) Pathways of influence of the Northern Hemisphere mid-high latitudes on East Asian climate: a review. Adv Atmos Sci 36:902–921

Li Y, Feng J, Li JP, Hu X (2019b) Equatorial windows and barriers for stationary Rossby wave propagation. J Clim 32:6117–6135

Li JP, Xie TJ, Tang XX, Wang H, Sun C, Feng J, Zheng F, Ding RQ (2021) Influence of the NAO on wintertime surface air temperature over the East Asia: multidecadal variability and decadal prediction. Adv Atmos Sci 39:625–642

Lin J, Wu B, Zhou T (2016) Is the interdecadal circumglobal teleconnection pattern excited by the Atlantic multidecadal Oscillation? Atmos Ocean Sci Lett 9:451–457

Liu YY, Wang L, Zhou W, Chen W (2014) Three Eurasian teleconnection patterns: spatial structures, temporal variability, and associated winter climate anomalies. Clim Dyn 42:2817–2839

Liu S, Wu Q, Wang L, Schroeder SR, Zhang Y, Yao Y, Hu H (2020) Modeled climate responses to realistic extremes of Northern Hemisphere Spring and Summer snow anomalies. J Clim 33(22):9905–9927

Matsumura S, Yamazaki K (2012) Eurasian subarctic summer climate in response to anomalous snow cover. J Clim 25(4):1305–1317

Matsumura S, Yamazaki K, Tokioka T (2010) Summertime land–atmosphere interactions in response to anomalous springtime

snow cover in northern Eurasia. J Geophys Res Atmos (1984–2012) 115(D20):D20107
Matsumura S, Yamazaki L, Sato T (2015) Role of Siberian land–atmosphere coupling in the development of the August Okhotsk High in 2008. J Meteorol Soc Jpn 93:229–244
Monerie P-A, Robson J, Dong B, Dunstone N (2017) A role of the Atlantic Ocean in predicting summer surface air temperature over North East Asia? Clim Dyn 51:473–491
Morice CP, Kennedy JJ, Rayner NA, Jones PD (2012) Quantifying uncertainties in global and regional temperature change using an ensemble of observational estimates: the HadCRUT4 dataset. J Geophys Res 117:D08101
Park TW, Jeong JH, Ho CH, Kim SJ (2008) Characteristics of atmospheric circulation associated with cold surge occurrences in East Asia: a case study during 2005/06 winter. Adv Atmos Sci 25(5):791–804
Park TW, Ho CH, Deng Y (2014) A synoptic and dynamical characterization of wave-train and blocking cold surge over East Asia. Clim Dyn 43(3):753–770
Qiao S, Feng G (2016) Impact of the December North Atlantic Oscillation on the following February East Asian trough. J Geophys Res 121:10074–10088
Rayner NA, Parker DE, Horton EB, Folland CK, Alexander LV, Rowell DP, Kent EC, Kaplan A (2003) Global analyses of sea surface temperature, sea ice, and night marine air temperature since the late nineteenth century. J Geophys Res 108:4407
Robinson DA, Estilow TW, Program NOAACDR (2012) NOAA Climate Data Record (CDR) of Northern Hemisphere (NH) Snow Cover Extent (SCE), version 1. NOAA Natl Cent Environ Inf
Robock A, Mu M, Vinnikov K, Robinson D (2003) Land surface conditions over Eurasia and Indian summer monsoon rainfall. J Geophys Res Atmos 108:4131
Saito K, Cohen J (2003) The potential role of snow cover in forcing interannual variability of the major Northern Hemisphere mode. Geo Res Lett 30(6):1302
Saito K, Yasunari T, Cohen J (2004) Changes in the sub-decadal covariability between Northern Hemisphere snow cover and the general circulation of the atmosphere. Int J Climatol 24(1):33–44
Screen JA, Simmonds I (2013) Exploring links between Arctic amplification and mid-latitude weather. Geophys Res Lett 40:959–964
Sun C, Li J, Zhao S (2015) Remote influence of Atlantic multidecadal variability on Siberian warm season precipitation. Sci Rep 5:16853
Sun Y, Li JP (2022) Synergistic effect of El Niño and the North Pacific Oscillation on wintertime precipitation over southeastern China and the East China Sea Kuroshio area. Clim Dyn 58:1635–1649
Takaya K, Nakamura H (2001) A formulation of a phase-independent wave activity flux for stationary and migratory quasi geostrophic eddies on a zonally varying basic flow. J Atmos Sci 58:608–627
Thompson DW, Wallace JM (1998) The Arctic Oscillation signature in the wintertime geopotential height and temperature fields. Geophys Res Lett 25:1297–1300
Thompson DW, Wallace JM (2000) Annular modes in the extratropical circulation. Part I: month-to-month variability. J Clim 13:1000–1016
Wallace JM, Gutzler DS (1981) Teleconnections in the geopotential height field during the Northern Hemisphere winter. Mon Weather Rev 109:784–812
Watanabe M, Kimoto M (2000) Atmosphere-ocean thermal coupling in the North Atlantic: a positive feedback. Q J R Meteorol Soc 126:3343–3369
Whitham G (1960) A note on group velocity. J Fluid Mech 9:347–352
Wu L, He F, Liu Z, Li C (2007) Atmospheric teleconnections of tropical Atlantic variability: interhemispheric, tropical–extratropical, and cross-basin interactions. J Clim 20:856–870
Wu R, Yang S, Liu S et al (2011) Northeast China summer temperature and North Atlantic SST. J Geophys Res 116:D16116
Wu B, Lin J, Zhou T (2016) Interdecadal circumglobal teleconnection pattern during boreal summer. Atmos Sci Lett 17:446–452
Xin X, Zhang L, Zhang J, Wu T, Fang Y (2013) Climate change projections over East Asia with BCC_CSM1.1 climate model under RCP scenarios. J Meteorol Soc Jpn 91(4):413–429
Ye KH, Lau NC (2019) Characteristics of Eurasian snowmelt and its impacts on the land surface and surface climate. Clim Dyn 52:1115–1138
Yin S, Feng J, Li JP (2013) Influences of the preceding winter Northern Hemisphere annular mode on the spring extreme low temperature events in the north of eastern China (in Chinese with English abstract). Acta Meteorol Sin 71(1):96–108
Zhang C, Wu R, Wang Z (2019) Impacts of summer North Atlantic sea surface temperature anomalies on the East Asian winter monsoon variability. J Clim 32(19):6513–6532
Zhao S, Li JP, Li Y (2015) Dynamics of an interhemispheric teleconnection across the critical latitude through a southerly duct during boreal winter. J Clim 28(19):7437–7456
Zhao S, Li JP, Li Y, Jin F-F, Zheng J (2019) Interhemispheric influence of Indo-Pacific convection oscillation on Southern Hemisphere rainfall through southward propagation of Rossby waves. Clim Dyn 52(5–6):3203–3221
Zhou J, Zuo Z, He Q (2021) Influence of Eurasian spring snowmelt on surface air temperature in late spring and early summer. J Clim 34(20):8191–8204